Research Article Vol. 3, No. 5/25 October 2025/Optica Quantum 480

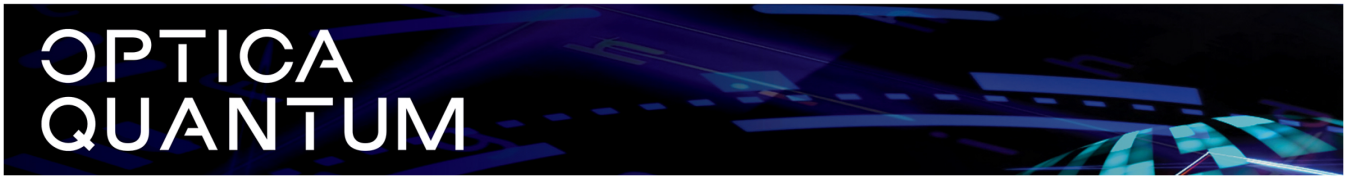

Entangling quantum memories at channel capacity

PRAJIT DHARA,[1,2,3,*] LIANG JIANG,[2,4] AND SAIKAT GUHA[1,2,3,5]

[1]Wyant College of Optical Sciences, The University of Arizona, Tucson, Arizona 85721, USA
[2]NSF-ERC Center for Quantum Networks, The University of Arizona, Tucson, Arizona 85721, USA
[3]Department of Electrical and Computer Engineering, University of Maryland, College Park, Maryland 20742, USA
[4]Pritzker School of Molecular Engineering, University of Chicago, Chicago, Illinois 60637, USA
[5]saikat@umd.edu
*prajitd@arizona.edu

Received 17 June 2025; revised 14 September 2025; accepted 19 September 2025; published 20 October 2025

Entangling quantum memories, mediated by optical-frequency or microwave channels, at high rates and fidelities is key for linking qubits across short and long ranges. All well-known protocols encode up to one qubit per optical mode, entangling one pair of memory qubits per transmitted mode over the channel, with probability η, the channel's transmissivity. The rate is proportional to η ideal Bell states (ebits) per mode. The quantum capacity, $C(\eta) = -\log_2(1-\eta)$ ebits per mode, which $\approx 1.44\eta$ for high loss, thereby making these schemes near rate-optimal. However, $C(\eta) \to \infty$ as $\eta \to 1$, making the known schemes highly rate-suboptimal for shorter ranges. We propose a cavity-assisted memory–photon interface that can be used to entangle matter memories with Gottesman–Kitaev–Preskill (GKP) photonic qudits, which, along with dual-homodyne entanglement swaps that retain analog information, enables entangling memories at capacity-approaching rates at low loss. We benefit from the loss resilience of GKP-encoded states and the ability to encode multiple qubits in one mode. Our memory–photon interface further supports the preparation of needed ancilla GKP qudits. We expect our result to spur research in low-loss, high-cooperativity cavity-coupled qubits with high-efficiency optical coupling and demonstrations of high-rate short-range quantum links.

https://doi.org/10.1364/OPTICAQ.570931

1. INTRODUCTION

Entanglement is a key enabling resource for many tasks in quantum-enhanced information processing [1,2]. The task of generating entanglement at high rates and high fidelity between multiple parties is a core challenge. The fundamental unit of an entanglement generation network is a single quantum link, connecting two parties over a lossy optical (or potentially microwave) frequency channel, often characterized by the channel's transmissivity η. The network may serve multiple qubits in a quantum processor, nodes of a metropolitan-scale quantum network, or quantum data centers separated by long distances [3]. The most prevalent protocols for generating heralded entanglement among qubits in quantum memories rely on quantum-optical modulation formats that encode up to one qubit per transmitted optical mode—thereby limiting entanglement generation to pairwise attempts per mode. If this attempt succeeds with probability proportional to η (e.g., when the dual-rail encoding is used [4,5]), the entanglement generation rate, $\mathcal{R} \propto \eta$ ideal Bell states per mode (ebits/mode). The maximum allowable entanglement rate with two-way authenticated classical communications assistance is the *quantum capacity* of the pure loss bosonic channel, given by: $C(\eta) = -\log(1-\eta)$ ebits/mode [6]. In the $\eta \ll 1$ (high loss) regime, known entanglement generation schemes are near rate-optimal as $C(\eta) \approx 1.44\eta$. However, as $\eta \to 1$ we note $C(\eta) \to \infty$, necessitating the encoding of multiple qubits in a single optical mode. This loss regime is applicable for intraprocessor and data center quantum links, local-area quantum networks, and potentially even long-haul networks relying on ultra-low loss transmission assisted by vacuum beam guides [7].

In this Letter, we propose and analyze a quantum link architecture that achieves the quantum channel capacity scaling in the $\eta \to 1$ regime. Our link proposal entangles N-qubit blocks of two remote memory registers, mediated by $d = 2^N$-dimensional photonic (qudit) encodings at rates approaching capacity at low channel loss. Our link utilizes the maximally entangled memory–photon entangled state of an N-qubit memory register (at each site) and a single optical mode encoding N qubits in the Gottesman–Kitaev–Preskill (GKP) photonic qu(d)it format [8]—which is realizable using a generalized cavity-assisted memory–photon interface for grid-like bosonic qubit encodings [9]. The optical qudits from each site undergo lossy propagation to a middle station where a dual-homodyne-based entanglement swap creates N qubit remote entanglement, with the measurement outcome assisting post-processing at the error correction stage [10,11]. When $\eta = 1$ and ideal memory–photon entangled states are utilized, our protocol generates N ebits per transmitted mode where N can be arbitrarily high, in congruence with the fact that $C(\eta) = \infty$ for $\eta = 1$. In the low-loss regime (η ap-

proaching 1), we show that the distillable entanglement rate achieved by the link approaches $C(\eta)$, within a constant separation of ~ 1 ebit/mode, outperforming known schemes by order of magnitude or more. This advantage is retained even with finite-squeezed GKP qudits—our proposal uses individual devices that have been demonstrated in isolation, hence making it an attractive candidate for near-future realizations.

Our scheme benefits from the resilience of GKP qudits to channel loss [12,13] and the GKP encoding's natural extension to accommodate multiple qubits in one mode. We show that even with 5-dB-squeezed GKP qubits, intra-processor entanglement rates can be doubled compared to single photon-based encoding and linear optical entanglement swap assisted links [4,5,9]. We anticipate our result to lead to more sophisticated protocols and practical demonstrations of high-rate short-range quantum links. The efficacy of the GKP encoding has potential for the development of error-corrected quantum memories for link-level entanglement generation [14]. Extensions of our protocol are applicable to a variety of research topics pertaining to hybrid continuous-discrete variable quantum logic gates and resource-efficient non-Gaussian photonic state preparation. Furthermore, developing low-loss high-cooperativity cavity-coupled qubits with high-efficiency optical coupling is a major experimental target, and our scheme will further catalyze this technology development.

2. BACKGROUND

We consider a single bosonic mode with the creation ($\hat{a}$) and annihilation ($\hat{a}^\dagger$) operators defined in terms of the canonical position ($\hat{q}$) and momentum ($\hat{p}$) as $\hat{a} = (\hat{q} + i\hat{p})/\sqrt{2}; \hat{a}^\dagger = (\hat{q} - i\hat{p})/\sqrt{2}$ (i.e., $\hbar = 1$ units). The logical *square-lattice GKP* (sq-GKP) qudit subspace [8,13] is the eigenspace formed by the displacement operators:

$$\begin{aligned} \hat{S}_q^{(d)} &= \exp(-i\sqrt{2\pi d}\hat{p}), \text{ and} \\ \hat{S}_p^{(d)} &= \exp(i\sqrt{2\pi d}\hat{q}). \end{aligned} \tag{1}$$

The logical basis states can be expressed in terms of position eigenstates as:

$$\mu_q \propto \sum_{n=-\infty}^{\infty} q = (dn + \mu_q)\sqrt{2\pi/d}, \tag{2}$$

where $\mu_q = 0, 1, \ldots, d-1 \equiv \mathrm{res}(d)$ viz. residue set of d. Hence, a position quadrature displacement of $j\sqrt{2\pi/d}$ maps states from $\mu_q \to \mu_q + j$, where we will drop the implicit modulo d for brevity. Physical approximations to the ideal (infinite and non-normalizable) GKP logical states can be made by imposing finite peak widths and/or phase envelopes; we use finite-squeezed physical approximations as random-Gaussian displacements of the ideal logical states:

$$\tilde{\mu}_q \propto \int du\, dv\, \Gamma(u,v)\ \exp(-iu\hat{p})\exp(iv\hat{q})\,\mu_q, \tag{3}$$

where $\Gamma(u,v)$ is a bivariate Gaussian distribution:

$$\Gamma(u,v) = \frac{1}{2\pi\sigma_u\sigma_v}\exp\left[-\frac{u^2}{2\sigma_u^2} - \frac{v^2}{2\sigma_v^2}\right], \tag{4}$$

where typically $\sigma_u^2 = \sigma_v^2 = \sigma^2$ ($\sigma^2 \to 0$ is the ideal qudit limit). This model allows us to analytically track the effect of channel loss and noise on GKP qudits by the evolution of error variance σ^2.

We model our *quantum memories* as N three-level (levels labelled by $0_M, 1_M, 2_M$) atomic systems each with a qubit subspace (0_M and 1_M) and a single coupled interaction at an optical frequency ($1_M \leftrightarrow 2_M$). Charged quantum dots [15,16], trapped ions [17], cold atoms [18], and solid-state vacancy centers [19–21] may support such a level structure in their energy manifold. Each atomic system is integrated in a single-mode cavity with one coupling port that couples the cavity mode ($\hat{a}_c$) with incoming ($\hat{a}_{\mathrm{in}}$) and outgoing ($\hat{a}_{\mathrm{out}}$) free-space optical modes at coupling rate κ_c; enabling the atom-photon controlled-phase rotation interaction CR_π [18,22], where,

$$CR_\pi = 00_M \otimes \hat{\mathbb{I}}_B + 11_M \otimes \hat{R}_B(\pi), \tag{5}$$

with $\hat{R}_B(\pi)$ denoting a π-phase rotation on the reflected travelling wave bosonic (optical) mode. The controlled phase rotation gate's performance is evaluated in terms of the system cooperativity, $C = 4g^2/(\kappa\gamma_m)$ and the cavity efficiency, $\zeta = \kappa_c/(\kappa_c + \kappa_l) \equiv \kappa_c/\kappa$, where g is the atom-cavity interaction strength, κ_l the cavity leakage rate, and γ_m the atomic decay rate. The ideal interaction necessitates virtual occupation of the excited state, i.e., $\langle 22_M - 11_M\rangle \approx -1$, which is achieved when atomic detuning $|\omega - \omega_a| \gg g\sqrt{\langle \hat{a}_c^\dagger \hat{a}_c\rangle}$. It is important to note that for $\langle \hat{a}_c^\dagger \hat{a}_c\rangle \sim 1$ (approximately one photon interacts with the atom), one can derive exact dynamical equations for the field and atomic operators [23] as well as input–output relations of bosonic mode operators ([9], overview in Section II of Supplement 1).

3. MEMORY REGISTER TO GKP QUDIT CSUM GATE PROTOCOL

We provide a brief overview of the CSUM gate interaction (depicted in Fig. 1)—we will use the symbols B_j, M_k, and G for the jth interacting bosonic mode, kth memory qubit, and bosonic mode excited in the GKP qudit basis state ($d = 2^N$), respectively, where both $j, k \in \{1, 2, \ldots, N\}$. We consider the CSUM gate from the memory register to sq-GKP qudits—the modifications for other hybrid two-qudit gates are specified in Supplement 1.

Without loss of generality, we consider an initial pre-displaced state $D((d-1)\sqrt{2\pi/d}/2)0_{q_G}$. ($D(\alpha) = \exp(\alpha\hat{a}_G^\dagger - \alpha^*\hat{a}_G)$ is the displacement operator for the bosonic mode excited in the GKP qudit state.) The memory register is initialized in the $\psi_{\boldsymbol{M}} = \bigotimes_{i=1}^{N} +_{M_i} = \frac{1}{\sqrt{d}}\sum_{\boldsymbol{m}=0}^{d-1} \boldsymbol{m}_{\boldsymbol{M}}$ state, where $\boldsymbol{m}$ is a shorthand for the decimal representation of the N bit binary string $m_N, m_{N-1}, \ldots, m_1$ for the joint-logical states of the memories ordered $M_N, M_{N-1}, \ldots, M_1$. The CSUM gate protocol requires three interaction:

(1) Reflect the coherent-states $\alpha_{k_{B_k}}$ off of corresponding the cavity-coupled memories M_k, where,

$$\alpha_k\sqrt{1-\zeta} = d \times 2^{-k-1}\sqrt{2\pi/d}.$$

(2) Sequentially displace the GKP qudit state using the reflected coherent states by beamsplitter interaction with reflectivity $\zeta \to 1$. The total memory-state dependent displacement effectively applies a controlled qudit Pauli gate on 0_G.

(3) Apply Pauli $\hat{X}$ gates on the memories, followed by a phase-nulling second cavity reflection of the bosonic modes. Reapply Pauli $\hat{X}$ gates on the memories.

Using the initial memory state $\psi_{\boldsymbol{M}} = \bigotimes_{i=1}^{N} +_{M_i}$ and $\varphi_G = 0_{q_G}$ results in the maximally entangled memory register-GKP qudit state:

$$\Psi_{\boldsymbol{M}G} = \frac{1}{\sqrt{d}} \sum_{m=0}^{d-1} \boldsymbol{m}_{\boldsymbol{M}} m_{q_G}, \tag{6}$$

which is equivalent to a CSUM gate (i.e., qudit CNOT gate).

The coherent state-assisted conditional (on memory state) displacement of the GKP qudit is the key feature of this protocol. Interaction of the coherent pulses with memories initialized in $\boldsymbol{m}_{\boldsymbol{M}}$ transforms the coherent states as:

$$\boldsymbol{m}_{\boldsymbol{M}} \otimes \left(\otimes_{k=1}^{N} \alpha_{k_{B_k}}\right) \to \boldsymbol{m}_{\boldsymbol{M}} \otimes \left(\otimes_{k=1}^{N} (-1)^{m_k+1} \alpha_{k_{B_k}}\right). \tag{7}$$

The net displacement ($\boldsymbol{S}_{\boldsymbol{m}}$) imparted by the sequential displacement can then be simplified to:

$$\begin{aligned} \boldsymbol{S}_{\boldsymbol{m}} &= \sum_{k=1}^{N} (-1)^{m_k+1} \alpha_k \sqrt{1-\zeta} = \sum_{k=1}^{N} (-1)^{m_k+1} \frac{d\sqrt{2\pi/d}}{2^{k+1}} \\ &= (\boldsymbol{m} - (d-1)/2) \times \sqrt{2\pi/d}. \end{aligned} \tag{8}$$

We note that the GKP state is predisplaced by $((d-1)/2)\sqrt{2\pi/d}$, resulting in the net displacement $\boldsymbol{S}'_{\boldsymbol{m}} = \boldsymbol{m}\sqrt{2\pi/d}$. For the d-dimensional analogue of the CZ gate, we may choose $\alpha_k e^{i\pi/2}$. Readers may look at the Table I in Supplement 1 for a detailed proof as well the choice of α_k for other hybrid two qudit gates.

4. EFFECT OF IMPERFECTIONS IN CAVITY-ASSISTED MEMORY-GKP CSUM GATE

The cavity-assisted memory-GKP CSUM gate protocol assumes ideal memory-dependent phase rotation of input coherent pulses; however, non-idealities in the cavity–photon interface will degrade the gate fidelity, and subsequently the performance of the capacity achieving quantum link. Primarily, ideal memory-dependent phase must be imparted while minimizing photon loss in the reflected bosonic pulse (either from imperfect cavity coupling or atomic-state decay). Any reflection phase imperfections result in effective Pauli errors (from imperfect displacements) and photon loss manifests as dephasing noise on the final state. For a general cavity–photon interface, the final state (with memories initialized in $\psi_{\boldsymbol{M}}$) is given as:

$$\rho_{\boldsymbol{M}G} \approx \frac{1}{d} \sum_{\boldsymbol{m},\boldsymbol{m}'=0}^{d-1} g_{\boldsymbol{m},\boldsymbol{m}'} \boldsymbol{m}\boldsymbol{m}'_{\boldsymbol{M}} D(\boldsymbol{\beta}_{\boldsymbol{m}'}) \rho_G D^{\dagger}(\boldsymbol{\beta}_{\boldsymbol{m}'}), \tag{9}$$

where the realistic conditional displacement is:

$$\boldsymbol{\beta}_{\boldsymbol{m}} = \sum_{j=1}^{N} r_{(m_j)} (-1)^{m_k+1} \alpha_j \sqrt{1-\zeta}. \tag{10}$$

Here, $r_{m_k} \in \mathbb{C}$, with $|r_{m_k}| \in [0,1]$, describes the memory dependent phase, and the coefficients $g_{\boldsymbol{m},\boldsymbol{m}'}$ are given by:

$$g_{\boldsymbol{m},\boldsymbol{m}'} = \delta_{\boldsymbol{m},\boldsymbol{m}'} + (1 - \delta_{\boldsymbol{m},\boldsymbol{m}'}) |\lambda_{\boldsymbol{m},\boldsymbol{m}'}|^2, \tag{11}$$

with $|\lambda_{\boldsymbol{m},\boldsymbol{m}'}|^2$ representing the effective dephasing due to photon loss and $\delta_{\boldsymbol{m},\boldsymbol{m}'}$ is the Kronecker delta symbol. For $C \gg 1$ and $|\omega - \omega_c| \to 0$, we may achieve the approximate relation $-r_0 \approx r_1 = 1$—any additional sources of loss can be incorporated in $|\lambda_{\boldsymbol{m},\boldsymbol{m}'}|^2$. For $r_0 \to 1$ and $r_1 \to -1$, the largest coherent pulse must satisfy the virtual excitation condition—we need the pulse length τ to satisfy $\tau \gg |\alpha_1|^2 = \pi d/16\kappa(1-\eta)$ (since α_1 has the largest magnitude [18,22]).

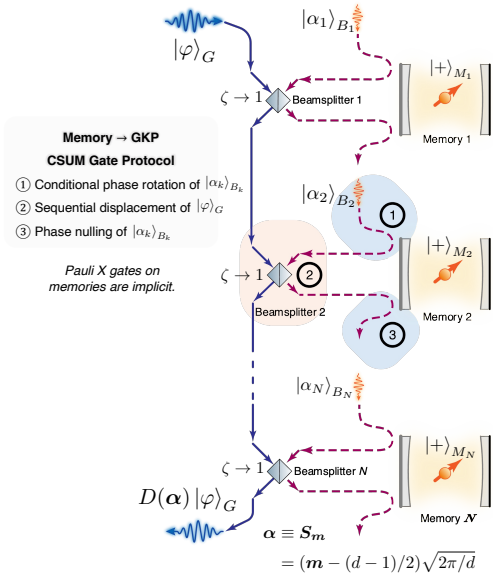

Fig. 1. Overview of the protocol implementing the CSUM gate, involving reflection of coherent pulses from a register of N-quantum memories integrated in cavities and memory-state dependent sequential displacement of pre-displaced GKP qudit states.

5. APPROACHING CHANNEL CAPACITY WITH QUDIT-ASSISTED ENTANGLEMENT SWAPS

With the assistance of the CSUM gate, we demonstrate a quantum link for entanglement generation over a pure loss bosonic channel (of transmissivity η) at rates approaching channel capacity. The midpoint swap link (Fig. 2(a)) connects two parties where each party locally generates the $\Psi_{\boldsymbol{M}_k G_k}; k = \{1,2\}$ state of their registers of N quantum memories and local GKP qudits. The GKP qudit modes are transmitted over the half-channels of transmissivities $\sqrt{\eta}$ to a central node, which performs a projective GKP qudit basis Bell state measurement (BSM) with a dual-homodyne measurement of the output modes after a balanced beamsplitter. In the midpoint source link (Fig. 2(b)), a central node generates maximally entangled GKP qudit Bell pairs, which are transmitted to the end users. The end users load the qudit on the memory register with a CSUM gate and qudit Pauli X basis measurement. In both link configurations, the measurements herald the generation of an entanglement state of the memory registers $\tilde{\rho}_{\boldsymbol{M}_1,\boldsymbol{M}_2}$, conditioned of the real-valued measurement outcomes (say x, y). One may already note that in principle we can choose d optimally to enable high-rate communications.

The effect of loss (with implicit pre-amplification of the state [13] or post-processing [11] of measurement outcomes) and finite-squeezing [24] on the GKP qudit states can be effectively modeled by a Gaussian random displacement channel on the ideal qudit states [11,13,25]. Given an initial state ρ_G, the random displacement channel $\mathcal{N}_{B_2}[\sigma^2]$ modifies the state as:

$$\mathcal{N}_{B_2}[\sigma^2](\rho_G) = \frac{1}{\pi\sigma^2} \int d^2\alpha \, e^{-|\alpha|^2/\sigma^2} D(\alpha) \rho D^{\dagger}(\alpha). \tag{12}$$

The random displacement channel acting on a general GKP-encoded qudit state does not directly map to a Pauli error channel—we analyze the effect of the random displacement channel using a standard Pauli twirling approach [26] making the achievable rate lower-bound calculable tractable.

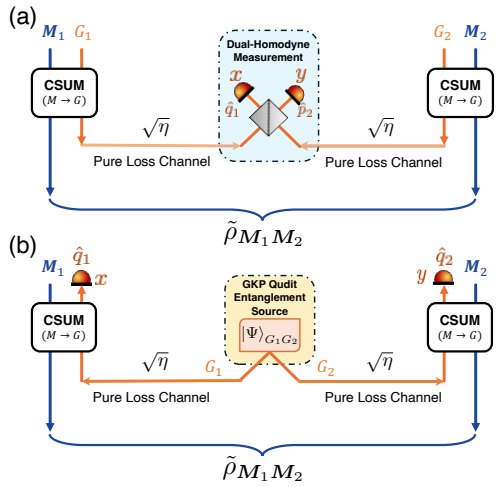

Fig. 2. Layout of quantum links for entanglement generation at channel capacity (a) Midpoint swap link configuration, where each party performs the CSUM gate on local memory registers $(\boldsymbol{M}_1, \boldsymbol{M}_2)$ and GKP qudit states (G_1, G_2) before transmission to the midpoint of a link (of transmissivity η) for a dual-homodyne measurement-based entanglement swap. (b) Midpoint source link configuration, where the central node generates a GKP qudit entangled state which is transmitted to the end-users; both users load the incoming GKP qubits (G_1, G_2) with CSUM gates and qudit X basis measurement. For both links, the measurement outcomes x, y, heralds the generation of an entangled state of the memory registers $(\tilde{\rho}_{\boldsymbol{M}_1,\boldsymbol{M}_2})$.

Let us assume that, as a virtue of possessing a perfect CSUM gate, ideal memories and ideal GKP qudits, both parties start with the ideal memory-GKP maximally entangled state:

$$\Psi_{0,0_{\boldsymbol{M}_i,G_i}} = \frac{1}{\sqrt{d}} \sum_{\boldsymbol{m},m=0}^{d-1} \boldsymbol{m}_{\boldsymbol{M}_i} m_{G_i}; i = \{1,2\}. \tag{13}$$

Lossless transmission, i.e., $\eta = 1$ yields a final state, $\Psi_{x_L,y_L\boldsymbol{M}_1,\boldsymbol{M}_2} \equiv W_1^{(0,d-x_L)} W_2^{(d-y_L,0)} \Psi_{0,0\boldsymbol{M}_1,\boldsymbol{M}_2}$, where x_L, $y_L \in \mathrm{res}(d)$ are the logical outcomes of the dual homodyne measurement, and $\{W_i^{(m,n)}\}; i = \{1,2\}, m, n \in \mathrm{res}(d)$ are the Weyl-operators on qudits (see Section I in Supplement 1 for definitions). Introducing any loss (even with ideal GKP states) yields a mixed state $\rho_{\boldsymbol{M}_1,\boldsymbol{M}_2}$. For physical GKP states of peak variance σ_i^2 transmission over a pure loss channel of transmissivity η modifies both σ_i^2 and the grid spacing. One may restore the grid spacing by pre-amplifying the transmitted state (applying an amplification channel of gain $G = 1/\eta$), or post-process the dual-homodyne measurement outcomes on a classical computer (*CC-amplification* [11]). The corresponding variance transformations are:

$$\text{Pre-amplification: } \sigma_i^2 \to \sigma_i^2 + (1-\eta) \tag{14a}$$

$$\text{CC-amplification: } \sigma_i^2 \to \sigma_i^2 + \frac{1-\eta}{2\eta}. \tag{14b}$$

We note that CC-amplification adds a smaller value of noise for all values of loss $\eta > 0.5$. To characterize the final state, we analyze the error probabilities for the twirled channel model. The probability of making k-shift errors in the logical measurement for sq-GKP states (along either the Pauli X or Z basis) is given by [13,27]:

$$P^{(\mathrm{sq})}(X^k, \sigma^2) \equiv P^{(\mathrm{sq})}(Z^k, \sigma^2)$$
$$= \sum_{j\in\mathbb{Z}} \frac{1}{2}\left[\mathrm{erf}\left(\sqrt{\frac{2\pi}{d}}\frac{jd+k+1/2}{\sigma}\right) - \mathrm{erf}\left(\sqrt{\frac{2\pi}{d}}\frac{jd+k-1/2}{\sigma}\right)\right], \tag{15}$$

where $k \in \{0, 1, 2, \ldots, d-1\}$. The summation over the index j accounts for shifts of magnitude greater than one lattice spacing of $\sqrt{2\pi d}$.

The "twirled" noise model (see Supplement 1 for details) allows us to approximate $\rho_{\boldsymbol{M}_1,\boldsymbol{M}_2}$ by the state:

$$\tilde{\rho}_{\boldsymbol{M}_1\boldsymbol{M}_2} = \sum_{k_1,k_2=0}^{d-1} P_{\mathrm{shift}}^{(k_1,k_2)}(\sigma^2)\, \Psi_{k'',l''}\Psi_{k'',l''\boldsymbol{M}_1\boldsymbol{M}_2}, \tag{16}$$

with shift error probability:

$$P_{\mathrm{shift}}^{(k_1,k_2)}(\sigma^2) = P^{(\mathrm{sq})}(X^{k_1}, \sigma^2) \cdot P^{(\mathrm{sq})}(Z^{k_2}, \sigma^2) \tag{17}$$

and $k'' = k' + k_1; l'' = l' + k_2$. An achievable lower bound to the distillable entanglement for $\tilde{\rho}_{\boldsymbol{M}_1\boldsymbol{M}_2}$ is given by the *hashing bound* [28],

$$I(\tilde{\rho}_{\boldsymbol{M}_1\boldsymbol{M}_2}) = \log_2(d) + \sum_{k_1,k_2=0}^{d-1} P_{\mathrm{shift}}^{(k_1,k_2)}(\sigma^2) \log_2 P_{\mathrm{shift}}^{(k_1,k_2)}(\sigma^2). \tag{18}$$

Further analysis in this article is limited to $\tilde{\rho}_{\boldsymbol{M}_1\boldsymbol{M}_2}$; we justify this in Section III of Supplement 1.

We plot the achievable hashing rate as function of $\sqrt{\eta}$, for memory registers sizes (N; varying colors) utilizing GKP qudits of appropriate dimension ($d = 2^N$) in Fig. 3 assuming the sq-GKP encoding for both the pre-amplification (Fig. 3(a)) and CC-amplification (Fig. 3(b)) protocols. The performance of infinite squeezed states (solid; $\sigma_i^2 \to 0$) is shown as a benchmark; finite squeezed states for 10 dB (dot-dashed; + markers) and 5 dB (dashed; ∘ markers) of squeezing are shown for comparison with the repeater-less channel capacity of $-\log_2(1-\sqrt{\eta})$ (black; dotted) [6].

For $\eta \to 0$ dB, we note that $\mathcal{R}(\tilde{\rho}_{\boldsymbol{M}_1\boldsymbol{M}_2}) \to N$ – increasing the qudit dimension enables rate scaling of $-\log_2(1-\sqrt{\eta})$ for $\eta \to 1$ (with an offset of $\log_2 e$ similar to Ref. [13]). CC-amplification (which adds lower variance noise) outperforms pre-amplification for all values of half channel loss upto 3 dB (as noted by the transformation rules earlier). Realistic implementations of the high-rate links will be affected by the CSUM gate imperfections as well as the finite squeezing of the GKP states—we defer a detailed examination of these effects to future works.

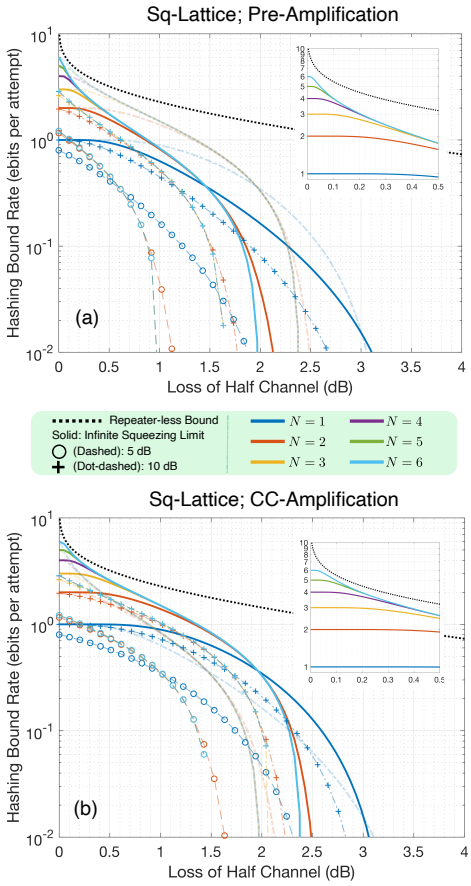

Fig. 3. Performance of the qudit-swap assisted link for N-qubit memory registers (varying colors) utilizing square lattice GKP qudit encodings ($d = 2^N$) assuming (a) pre-amplification of the transmitted qudits, and (b) CC-amplification of the dual homodyne measurement outcomes. We analyze the performance of protocol for infinite squeezed states (solid), 5 dB (dashed; ∘ markers) and 10 dB (dot-dashed; + markers) squeezed states with the channel capacity of $C(\eta)$.

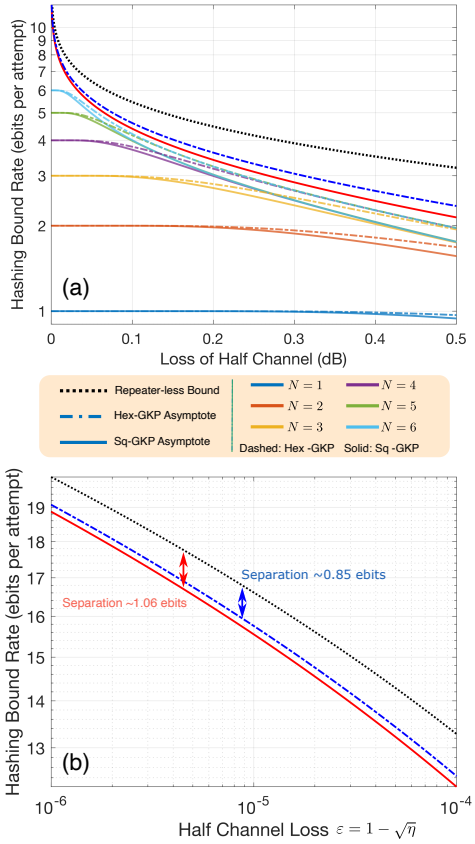

Fig. 4. Low-loss limit performance of the qudit-swap assisted link. (a) Comparison of varying N (varying colors) utilizing sq-GKP (solid lines) and hex-GKP (dot-dashed) qudit encodings ($d = 2^N$) for the pre-amplification protocol. We compare the finite squeezing, finite encoding size performance with calculated asymptotic rate scaling (red: sq-GKP; blue: hex-GKP) and the repeater-less channel capacity of $Q_2(\eta) = -\log_2(1-\sqrt{\eta})$ (black, dotted). (b) Comparison of the asymptotic expressions (for either protocol) and the repeater-less bound showing a finite separation in the extremely low-loss regime, i.e., $\varepsilon \to 0; \eta \to 1$.

We also find that achievable hashing rate approaches $C(\sqrt{\eta}) =$ as $\eta \to 1$ as $d \to \infty$ and $\sigma^2 = 0$. Our proof is outlined as follows (details in Section III of Supplement 1)—in the limit $\sigma^2 \to 0$ it is sufficient to lower bound $P^{(\mathrm{sq/hex})}(X^k/Z^k, \sigma^2)$ by dropping the summation over the lattice positions and only considering $|k| \leq 1$, i.e., the probability of incurring larger (greater than one shift) logical errors is negligible. Carrying out a Taylor expansion of the probability of shift error for $d \to \infty$ and $\eta \to 1$, gives us the simplified expressions:

$$\tilde{P}^{(\mathrm{sq})}_{\mathrm{shift}}(0;\varepsilon) = 1 - \frac{\sqrt{2d\varepsilon}\exp\left(-\pi/(2d\varepsilon)\right)}{\pi}$$
$$\tilde{P}^{(\mathrm{sq})}_{\mathrm{shift}}(\pm 1;\varepsilon) = \frac{\sqrt{d\varepsilon}\exp\left(-\pi/(2d\varepsilon)\right)}{\sqrt{2}\pi}, \quad (19)$$

where $\varepsilon = 1 - \sqrt{\eta}$ for the pre-amplification protocol. Intuitively, $2d\varepsilon$ is the effective variance of the logical measurement error distribution—to attain channel capacity scaling for $\varepsilon \to 0$, the qudit dimension must grow commensurate to ε. We may then make the ansatz that $2d\varepsilon$ is some real constant ξ and derive a lower bound $I_{\mathrm{LB}}(\xi)$ to $I(\tilde{\rho}_{\boldsymbol{M}_1\boldsymbol{M}_2})$. This ansatz matches the expectation that the qudit dimension grows as $\eta \to 1$; the optimal ξ will yield the best rate scaling, or, minimize the difference $C(\sqrt{\eta}) - I_{\mathrm{LB}}(\xi)$. We numerically optimize ξ (via the Newton-Raphson method) to obtain $\xi_{\mathrm{opt}} \approx 1.642$, which yields a separation of $C(\sqrt{\eta}) - I_{\mathrm{LB}}(\xi) \approx 1.06$ ebits/ch. A similar ansatz can be made for the CC-amplification where $\sqrt{\eta} = 1 - \varepsilon \Rightarrow (1 - \sqrt{\eta})/(2\sqrt{\eta}) \approx \varepsilon/2$. Then by choosing $d\varepsilon = \xi_{\mathrm{opt}}$ we obtain the same scaling as that of the pre-amplification protocol.

Similarly for the CC-amplification, the ansatz $\sqrt{3}d\varepsilon/2 = \xi'_{\mathrm{opt}}$ yields the required rate scaling. We compare the low-loss achievable rate vs. $\sqrt{\eta}$ for varying N (varying colors) for both the sq-GKP (solid) and hex-GKP (dot-dashed) encodings, with their corresponding low-loss asymptotic curves in Fig. 4. In Fig. 4(b), we compare the asymptotic rate expressions with the repeater-less channel capacity and show the finite separation as predicted by our expressions.

6. UTILIZING HEXAGONAL LATTICE GKP CODES

Hexagonal lattice GKP codes are a natural alternative to the square lattice codes discussed in the main text. The hex-GKP

qudits are defined as the eigenspace of the displacement operators:

$$\hat{S}_q^{(d)} = \exp\left[i\sqrt{2\pi d}\left(2/\sqrt{3}\right)^{1/2}(\hat{q}+\hat{p}/2)\right], \text{ and}$$
$$\hat{S}_p^{(d)} = \exp\left[-i\sqrt{2\pi d}\left(2/\sqrt{3}\right)^{1/2}(\sqrt{3}\hat{p}/2)\right]. \tag{20}$$

As with the sq-GKP, the ideal hex-GKP qudit states are unphysical—normalized versions can be derived by considering finite peak variances, as prescribed in Eq. (3). As a result of the modified phase space distribution, the pre-displacements and coherent pulse amplitudes for the memory-GKP CSUM gate protocol must be suitably adapted.

The quantum link architecture for entanglement generation remains unmodified—for hex-GKP states, the error probabilities (in the heralded state, Eq. (15)) are modified as:

$$P^{(\text{hex})}(X^k,\sigma^2) \equiv P^{(\text{hex})}(Z^k,\sigma^2)$$
$$= \sum_{j\in\mathbb{Z}} \frac{1}{2}\left[\text{erf}\left(\sqrt{\frac{2\pi}{d}}\frac{jd+k+1/2}{\sigma(\sqrt{3}/2)^{1/2}}\right) - \text{erf}\left(\sqrt{\frac{2\pi}{d}}\frac{jd+k-1/2}{\sigma(\sqrt{3}/2)^{1/2}}\right)\right]. \tag{21}$$

Accordingly, the rest of analysis for the quantum links is similar to the sq-GKP encoding. We plot the achievable hashing rate as function of $\sqrt{\eta}$, for memory registers sizes (N; varying colors) utilizing hex-GKP qudits of appropriate dimension ($d=2^N$) in Fig. 5 for both the pre-amplification (Fig. 5(a)) and CC-amplification protocols (Fig. 5(b)).

Similar to the sq-GKP, we find that achievable hashing rate approaches $C(\sqrt{\eta})$ as $\eta\to 1$ as $d\to\infty$ and $\sigma^2=0$. Mirroring the previous approach, in the limit $\sigma^2\to 0$ it is sufficient to lower bound $P^{(\text{hex})}(X^k/Z^k,\sigma^2)$ by only considering $|k|\le 1$. For hex-GKP qudits, the larger separation between the peaks of the logical states ($\sim\sqrt{4\pi/\sqrt{3}d}$) yields a lower Pauli error probability. Assuming single shift errors, the appropriate Taylor series expansion of the errors gives us:

$$\tilde{P}^{(\text{hex})}_{\text{shift}}(0;\varepsilon) = 1 - \frac{\sqrt{\sqrt{3}d\varepsilon}\exp\left(-\pi/(\sqrt{3}d\varepsilon)\right)}{\pi};$$
$$\tilde{P}^{(\text{hex})}_{\text{shift}}(\pm 1;\varepsilon) = \frac{\sqrt{\sqrt{3}d\varepsilon}\exp\left(-\pi/(\sqrt{3}d\varepsilon)\right)}{2\pi}. \tag{22}$$

Here, an ansatz of $\sqrt{3}d\varepsilon=\xi'$ with $\xi'_{\text{opt}}\approx 1.422$ minimizes $C(\sqrt{\eta})-I_{\text{LB}}\sim 0.85$ ebits/ch, matching the expectation that $\xi_{\text{opt}}/\xi'_{\text{opt}}=\sqrt{3}/2$, i.e., the qudit dimension vs. loss scaling is proportional to the improvement in the error probability between the lattice choices.

7. OUTLOOK

We have presented a method for generating entanglement between a register of N-quantum memories and $d=2^N$ dimensional GKP qudit states, assisted by the interaction of bosonic modes with cavity QED systems. We demonstrated how the resource states generated by our protocol could be utilized for the implementation of high-rate quantum links especially in the low-loss regime of operation, thereby highlighting a pathway to achieving channel capacity saturating quantum communication links.

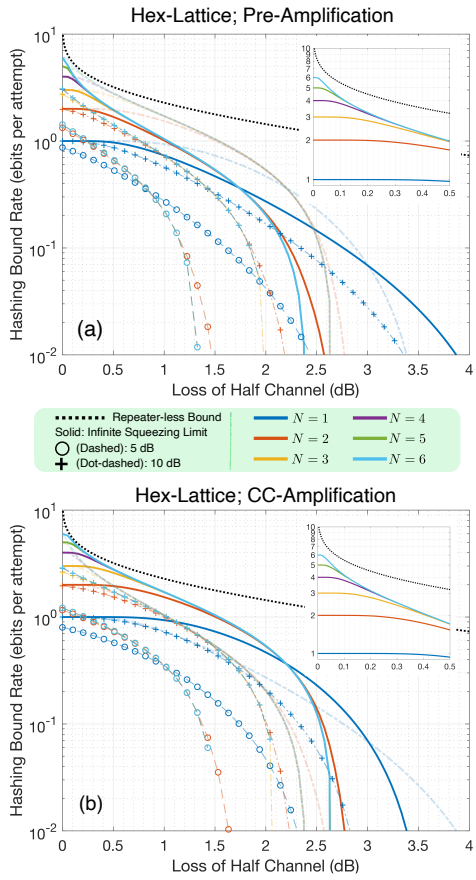

Fig. 5. Performance of the qudit-swap assisted link for N-qubit memory registers (varying colors) utilizing hexagonal lattice GKP qudit encodings ($d=2^N$) assuming (a) pre-amplification of the transmitted qudits, and (b) CC-amplification of the dual homodyne measurement outcomes. We analyze the performance of protocol for infinite squeezed states (solid), 5 dB (dashed; ∘ markers) and 10 dB (dot-dashed; + markers) squeezed states with the channel capacity of $C(\eta)$.

Furthermore, we show that the achievable entanglement generation rate scales as the repeaterless bound $C(\eta)$ for entanglement swapping in the low-loss regime with commensurately chosen N. State-of-the-art systems have demonstrated internal cooperativities of the order ~100. Improved cavity designs with larger cooperativities are being actively pursued in the various physical platforms that could support the necessary interactions. Coupled with efforts for large scale integration of physical quantum memory systems [29], the protocols suggested here could be achievable in the near term.

The CSUM gate protocol proposed in this work is a key element for hybrid quantum logic between memory registers and GKP qudits—the applications proposed in Ref. [9] can naturally be extended to high dimensional encodings. It is pertinent to note that protocols with higher-dimensional encodings are expected to be more sensitive to any imperfections in the cavity–photon interface. Further investigations of the underlying trade-offs and thresholds in the protocol performance are left for future works.

Funding. Directorate for Engineering (1941583); U.S. Department of Energy (1941583).

Acknowledgment. The authors would like to thank Filip Rozpedek, Kaushik P. Seshadreesan, Christos N. Gagatsos, Aileen Zhai, and Isack Padilla for fruitful discussions and comments on the manuscript. P.D. and S.G. acknowledge the Mega Qubit Router (MQR) project funded under federal support via a subcontract from the University of Arizona Applied Research Corporation (UA-ARC) for supporting this research. Additionally, all authors acknowledge the Engineering Research Center for Quantum Networks (CQN), awarded by the NSF and DoE under cooperative agreement number 1941583, for synergistic research support. L.J. additionally acknowledges support from the AFOSR MURI (FA9550-19-1-0399, FA9550-21-1-0209, FA9550-23-1-0338), DARPA (HR0011-24-9-0359, HR0011-24-9-0361), NSF (OMA-1936118, OMA-2137642, OSI-2326767, CCF-2312755), NTT Research, Packard Foundation (2020-71479), and the Marshall and Arlene Bennett Family Research Program.

Disclosures. The authors declare no conflicts of interest.

Data availability. No data were generated or analyzed in the presented research.

Supplemental document. See Supplement 1 for supporting content.

REFERENCES

1. H. J. Kimble, "The quantum internet," Nature **453**, 1023–1030 (2008).
2. K. Azuma, S. E. Economou, D. Elkouss, *et al.*, "Quantum repeaters: from quantum networks to the quantum internet," Rev. Mod. Phys. **95**, 045006 (2023).
3. L. M. Duan, M. D. Lukin, J. I. Cirac, *et al.*, "Long-distance quantum communication with atomic ensembles and linear optics," Nature **414**, 413–418 (2001).
4. S. D. Barrett and P. Kok, "Efficient high-fidelity quantum computation using matter qubits and linear optics," Phys. Rev. A **71**, 060310 (2005).
5. P. Dhara, D. Englund, and S. Guha, "Entangling quantum memories via heralded photonic bell measurement," Phys. Rev. Research **5**, 033149 (2023).
6. S. Pirandola, R. Laurenza, C. Ottaviani, *et al.*, "Fundamental limits of repeaterless quantum communications," Nat. Commun. **8**, 15043 (2017).
7. Y. Huang, F. Salces-Carcoba, R. X. Adhikari, *et al.*, "Vacuum beam guide for large-scale quantum networks," Phys. Rev. Lett. **133**, 020801 (2023).
8. D. Gottesman, A. Kitaev, and J. Preskill, "Encoding a qubit in an oscillator," Phys. Rev. A **64**, 012310 (2001).
9. P. Dhara, L. Jiang, and S. Guha, "Interfacing Gottesman-Kitaev-Preskill qubits to quantum memories," Phys. Rev. A **112**, 012401 (2025).
10. B. W. Walshe, B. Q. Baragiola, R. N. Alexander, *et al.*, "Continuous-variable gate teleportation and bosonic-code error correction," Phys. Rev. A **102**, 062411 (2020).
11. K. Fukui, R. N. Alexander, and P. van Loock, "All-optical long-distance quantum communication with Gottesman-Kitaev-Preskill qubits," Phys. Rev. Research **3**, 033118 (2021).
12. V. V. Albert, K. Noh, K. Duivenvoorden, *et al.*, "Performance and structure of single-mode bosonic codes," Phys. Rev. A **97**, 032346 (2018).
13. K. Noh, V. V. Albert, and L. Jiang, "Quantum capacity bounds of Gaussian thermal loss channels and achievable rates with Gottesman-Kitaev-Preskill codes," IEEE Trans. Inf. Theory **65**, 2563–2582 (2019).
14. S. Häussler and P. van Loock, "Quantum repeaters based on stationary Gottesman-Kitaev-Preskill qubits," Phys. Rev. A **111**, 062611 (2025).
15. D. Najer, I. Söllner, P. Sekatski, *et al.*, "A gated quantum dot strongly coupled to an optical microcavity," Nature **575**, 622–627 (2019).
16. Z. Luo, S. Sun, A. Karasahin, *et al.*, "A spin-photon interface using charge-tunable quantum dots strongly coupled to a cavity," Nano Lett. **19**, 7072–7077 (2019).
17. J. Schupp, V. Krcmarsky, V. Krutyanskiy, *et al.*, "Interface between trapped-ion qubits and traveling photons with close-to-optimal efficiency," PRX Quantum **2**, 020331 (2021).
18. L.-M. Duan and H. J. Kimble, "Scalable photonic quantum computation through cavity-assisted interactions," Phys. Rev. Lett. **92**, 127902 (2004).
19. M. K. Bhaskar, R. Riedinger, B. Machielse, *et al.*, "Experimental demonstration of memory-enhanced quantum communication," Nature **580**, 60–64 (2020).
20. P.-J. Stas, Y. Q. Huan, B. Machielse, *et al.*, "Robust multi-qubit quantum network node with integrated error detection," Science **378**, 557–560 (2022).
21. C. M. Knaut, A. Suleymanzade, Y.-C. Wei, *et al.*, "Entanglement of nanophotonic quantum memory nodes in a telecom network," Nature **629**, 573–578 (2024).
22. B. Hacker, S. Welte, S. Daiss, *et al.*, "Deterministic creation of entangled atom—light Schrödinger-cat states," Nat. Photonics **13**, 110–115 (2019).
23. M. G. Raymer, C. Embleton, and J. H. Shapiro, "The Duan-Kimble cavity-atom quantum memory loading scheme revisited," arXiv (2024).
24. K. P. Seshadreesan, P. Dhara, A. Patil, *et al.*, "Coherent manipulation of graph states composed of finite-energy Gottesman-Kitaev-Preskill-encoded qubits," Phys. Rev. A **105**, 052416 (2022).
25. F. Schmidt and P. van Loock, "Quantum error correction with higher Gottesman-Kitaev-Preskill codes: minimal measurements and linear optics," Phys. Rev. A **105**, 042427 (2022).
26. K. Fukui, A. Tomita, A. Okamoto, *et al.*, "High-threshold fault-tolerant quantum computation with analog quantum error correction," Phys. Rev. X **8**, 021054 (2018).
27. F. Schmidt, D. Miller, and P. van Loock, "Error-corrected quantum repeaters with Gottesman-Kitaev-Preskill qudits," Phys. Rev. A **109**, 042427 (2024).
28. I. Devetak and A. Winter, "Distillation of secret key and entanglement from quantum states," Proc. Math. Phys. Eng. Sci. **461**, 207–235 (2005).
29. N. H. Wan, T.-J. Lu, K. C. Chen, *et al.*, "Large-scale integration of artificial atoms in hybrid photonic circuits," Nature **583**, 226–231 (2020).